

HIGH-EFFICIENCY PHOTOSPHERIC EMISSION OF LONG-DURATION GAMMA-RAY BURST JETS: THE EFFECT OF THE VIEWING ANGLE

DAVIDE LAZZATI¹, BRIAN J. MORSONY², MITCHELL C. BEGELMAN^{3,4}

Draft version November 5, 2018

ABSTRACT

We present the results of a numerical investigation of the spectra and light curves of the emission from the photospheres of long-duration gamma-ray burst jets. We confirm that the photospheric emission has high efficiency and we show that the efficiency increases slightly with the off-axis angle. We show that the peak frequency of the observed spectrum is proportional to the square root of the photosphere's luminosity, in agreement with the Amati relation. However, a quantitative comparison reveals that the thermal peak frequency is too small for the corresponding total luminosity. As a consequence, the radiation must be out of thermal equilibrium with the baryons in order to reproduce the observations. Finally, we show that the spectrum integrated over the emitting surface is virtually indistinguishable from a Planck law, and therefore an additional mechanism has to be identified to explain the non-thermal behavior of the observed spectra at both high and low frequencies.

Subject headings: Gamma-ray burst: general — radiation mechanisms: thermal — methods: numerical — relativistic processes

1. INTRODUCTION

Despite more than thirty years of investigation, the origin of the prompt emission of GRBs is still veiled in mystery. Among the various proposed radiation mechanisms are synchrotron emission either in a baryon- or magnetically dominated jet (Piran 1999; Lloyd & Petrosian 2000; Zhang & Yan 2010), synchrotron self-Compton emission (Pe'er & Waxman 2004; Baring & Braby 2004), quasi-thermal comptonization (Ghisellini & Celotti 1999), bulk Compton emission (Lazzati et al. 2000), and photospheric emission, i.e., the radiation advected by the outflow that is released as the flow becomes optically thin (Goodman 1986; Rees & Meszaros 2005; Pe'er et al. 2005, 2006; Giannios 2006; Lazzati et al. 2009).

In recent years, the photospheric model has gained consensus for its robust modeling, its lacking of any adjustable parameters, its high efficiency (Lazzati et al. 2009, hereafter paper I; Mizuta et al. 2010; Nagakura et al. 2010) and its ability to easily reproduce the observed peak frequency (Pe'er et al. 2005, 2006; paper I). Theoretical investigation has moreover revealed that in the case of sub-photospheric dissipation, photospheric radiation is characterized by prominent non-thermal high-frequency tails, due to inverse Compton (IC) scattering of the thermal photons off relativistic electrons (Pe'er et al. 2006; Giannios 2006; Giannios & Spruit 2007; Lazzati & Begelman 2010). However, due to the relatively small size of their emission region, photospheric models cannot explain the very high frequency emission observed by Fermi (Abdo et al. 2009; Zhang et al. 2010). GeV photons cannot be produced in photospheric models and their origin has to be identified with the early afterglow (or external shock) emission (Kumar & Barniol Duran 2009; Ghisellini et al. 2010). In addition, photospheric models cannot naturally reproduce

the non-thermal low-frequency power-law spectra below the peak (see, e.g., Pe'er & Ryde 2010).

In this paper we present an extension of the simulations and results of Paper I. We have performed a simulation in a 10 times larger box, extending to 2.5×10^{13} cm, allowing us to explore the properties of the off-axis emission and to perform a quantitative comparison of our light curves and spectra with observational data. We also address the issue of the low-frequency spectrum which is observed to be non-thermal (Kaneko et al. 2006) but is predicted, in the simple thermal-photosphere model, to be thermal. In particular we explore whether the superposition of spectra of different temperatures over the emitting surface can significantly alter the thermal appearance of the spectrum (Pe'er & Ryde 2010).

This paper is organized as follows: in Sect. 2 we describe our simulations, in Sect. 3 we show the light curves and spectra extracted from our simulations, in Sect. 4 we compare our synthetic light curves and spectra to the Amati relation, and in Sect. 5 we discuss our results in the context of theoretical predictions and simulations from other groups.

2. NUMERICAL SIMULATIONS

The numerical simulation on which this paper is based is an extension of the one presented in paper I. A jet with luminosity $L = 5.33 \times 10^{50}$ erg/s is injected in the core of a 16 solar mass Wolf-Rayet star evolved to pre-explosion (model 16TI, Woosley & Heger 2006). The central engine has a constant luminosity for 100 s, after which it is sharply turned off. The jet is injected at a distance of 10^9 cm from the star center with an opening angle $\theta_0 = 10^\circ$, a Lorentz factor $\Gamma_0 = 5$, and enough internal energy to reach an asymptotic Lorentz factor $\Gamma_\infty = 400$, upon complete non-dissipative acceleration. The jet evolution was computed with the special-relativistic, adaptive mesh refinement code FLASH (Fryxell et al. 2000), as modified by the authors (Morsony et al. 2007) in a box of size 2.6×10^{13} cm in the jet direction and 5×10^{12} cm in the equatorial direction. Science frames were extracted every 0.2 seconds. The physics included, the resolution, and the refinement schemes were analogous to those of Morsony et al.

¹ Department of Physics, NC State University, 2401 Stinson Drive, Raleigh, NC 27695-8202

² Department of Astronomy, University of Wisconsin-Madison, 2535 Sterling Hall, 475 N. Charter Street, Madison WI 53706-1582

³ JILA, University of Colorado, 440 UCB, Boulder, CO 80309-0440

⁴ University of Colorado, Department of Astrophysical and Planetary Sciences, 389 UCB, Boulder, CO 80309-0389

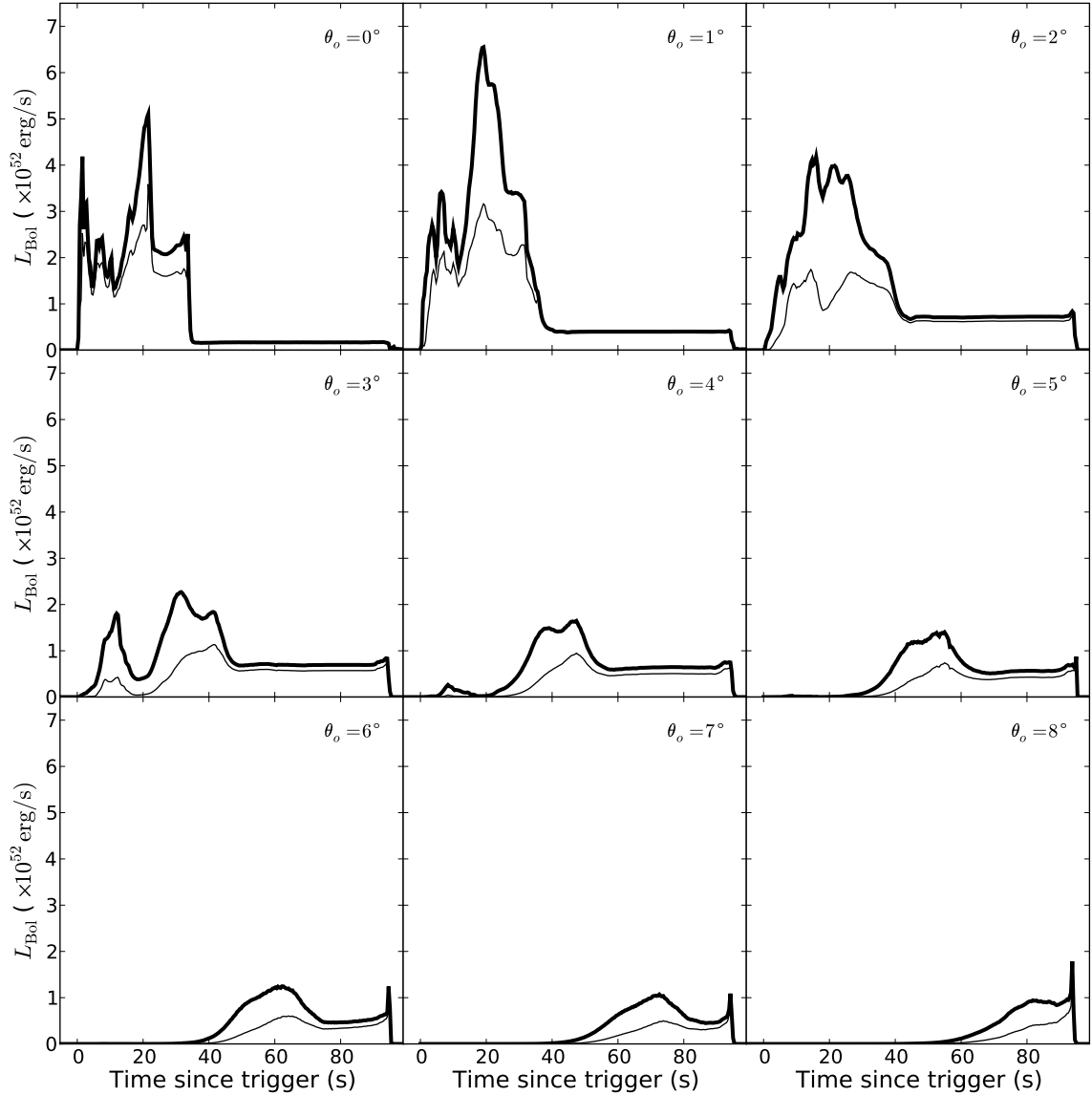


FIG. 1.— Photospheric light curves for different viewing angles. Thick lines show light curves obtained directly from the simulations, while thin lines show light curves when a correction for the finite size of the simulations box is applied (see text).

(2007) and paper I.

3. PHOTOSPHERIC LIGHT CURVES

The location of the photosphere in the observer direction (which we define as the z axis) Z_{ph} was calculated analogously to paper I by back-integrating the optical depth in space and time from a virtual observer located at a distance of $Z_{\text{obs}} = 1.3 \times 10^{13}$ cm. For each time step in the observer frame, the path of a photon is traced back in time as the photon travels in the evolving density and velocity patterns. As a result the location of the photosphere is computed as a function of the observed time, and no transformation from laboratory to observed coordinates is required. Note also that we use a Cartesian coordinate z for the photosphere rather than the radial distance r in order to automatically take into account the curvature effect and the equal arriving time surfaces. Let x and y be Cartesian coordinates in the plane perpendicular to the line of sight and z be the Cartesian coordinate along the line of sight. We define x to be the coordinate in the simulation plane and y the coordinate perpendicular to the simulation plane (and to the line of sight). Given the calculated

comoving density distribution $n'(t_{\text{lab}}, x, z)$, the location of the photosphere for the photons observed at the time t_{obs} and at a location x is given by:

$$1 = - \int_{Z_{\text{obs}}}^{Z_{\text{ph}}(x)} \sigma_T n' \left(t_{\text{obs}} - \frac{Z_{\text{obs}} - z}{c}, x, z \right) \Gamma [1 - \beta \cos(\theta_v)] dz \quad (1)$$

where $\beta \equiv \beta(t_{\text{lab}}, x, z)$ is the local velocity of the outflow in units of the speed of light, $\Gamma \equiv \Gamma(t_{\text{lab}}, x, z)$ is the local bulk Lorentz factor, and $\theta_v \equiv \theta_v(t_{\text{lab}}, x, z)$ is the angle between the velocity vector and the direction of the line of sight. All the values of β , Γ , and θ_v are evaluated at the same delayed coordinate $(t_{\text{lab}}, x, z) \equiv (t_{\text{obs}} - \frac{Z_{\text{obs}} - z}{c}, x, z)$ as the comoving density. Note that when off-axis calculations are performed (i.e., when the line of sight and the jet axis do not coincide), the photosphere location becomes a function of x and y and the above equation should be re-written with the explicit dependence on y as well as on x .

Once the photosphere's coordinate Z_{ph} is obtained, we compute the light curves as (paper I⁵)

$$L(t_{\text{obs}}) = \frac{ac}{2} \int_{-x_{\text{max}}}^{x_{\text{max}}} \int_{-y_{\text{max}}}^{y_{\text{max}}} dx dy \frac{T'^4}{(1 - \beta \cos \theta_v)^2} \quad (2)$$

where $T' = (3p/a)^{1/4}$ is the comoving temperature, $a = 7.56 \times 10^{-15} \text{ erg cm}^{-3} \text{ K}^{-4}$ is the radiation constant, and x_{max} is a distance perpendicular to the line of sight large enough so that the contribution to the emission at x_{max} is negligible. y_{max} satisfies the same constraint as x_{max} . Finally, the peak frequency of the observed spectrum is computed as

$$h\nu_{\text{peak}} = 2.8\delta k_B T' \quad (3)$$

where $\delta = 1/\Gamma(1 - \beta \cos \theta_v)$ is the Doppler factor.

In principle, one would want the observer location Z_{obs} to be approaching infinite, but practical considerations force it to be inside the computational area. This has the effect of biasing the photospheric distance, making it smaller than it should be. Assuming that the evolution at radii larger than the calculated photosphere is self similar and that there is no further acceleration, one can easily evaluate the correction thanks to the fact that the opacity in a wind scales as the inverse square of the distance. Simple algebra yields:

$$\frac{Z_{\text{ph,true}}}{Z_{\text{ph,sim}}} = \frac{1}{1 - Z_{\text{ph,sim}}/Z_{\text{obs}}} \quad (4)$$

where $Z_{\text{ph,true}}$ is the true location of the photosphere and $Z_{\text{ph,sim}}$ is the photospheric radius evaluated from a simulation with observer location Z_{obs} . Not surprisingly, the correction is small for $Z_{\text{ph,sim}} \ll Z_{\text{obs}}$, but for $Z_{\text{ph,sim}} = Z_{\text{obs}}/2$ the correction is not negligible. Under the same assumption of non-accelerating self-similar expansion, a correction for the light curve and peak frequency can be obtained, taking into account that the photon-to-baryon ratio does not change with distance (e.g., Lazzati & Begelman 2010) and that the photon temperature scales as $r^{-2/3}$ (e.g., Meszaros & Rees 2000). The true photospheric luminosity can be computed as:

$$L_{\text{true}} = L_{\text{sim}} (1 - Z_{\text{ph,sim}}/Z_{\text{out}})^{2/3} \quad (5)$$

⁵ Note that this equation is more precise than the one reported in paper I where the integration is erroneously performed over an angular direction rather than a linear one. It is also generalized to include lack of any axial symmetry, as is the case when the jet axis and the line of sight do not coincide.

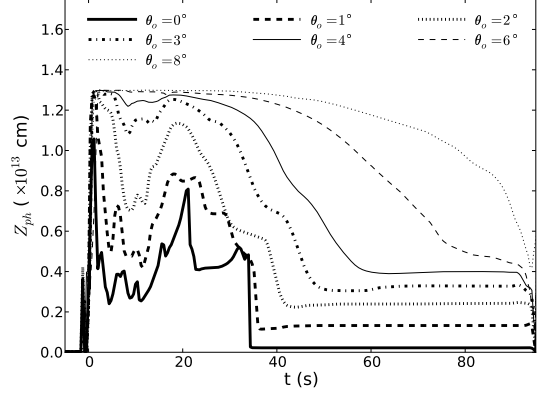


FIG. 2.— Photospheric distance for the lines of sight analyzed in this paper. The photospheric distance is shown for the $(x, y) = (0, 0)$ location, i.e., along the line of sight. Since the distance of the virtual observer is $Z_{\text{obs}} = 1.3 \times 10^{13} \text{ cm}$, all the photospheric distances that are measured to be close to Z_{obs} are likely affected by the finite size of the box (cfr. Eq. 4).

and the photon frequency analogously scales as:

$$\nu_{\text{true}} = \nu_{\text{sim}} (1 - Z_{\text{ph,sim}}/Z_{\text{out}})^{2/3} \quad (6)$$

Figure 1 shows the results of the light curve calculation at nine different observer angles $\theta_o = 0, 1, 2, 3, 4, 5, 6, 7$, and 8 degrees. The light curves at $\theta_o = 2.5$ and 3.5° were computed as well but are not shown in the figure. Light curves at $\theta_o > 8^\circ$ were not computed because the photospheric radius turned out to be too close to the outer boundary of the simulation box (see Figure 2 where all the photospheric radii are shown). Thick solid lines show the light curves as calculated from the simulations (Eq. 2) while thin lines show the light curves once the correction for the finite size of the box is applied (Eq. 5). The comparison between the thick and thin lines shows that the correction is not large, mostly a factor 2, but becomes progressively more important at large off-axis angles. The figure confirms the results of our paper I (see also Mizuta et al. 2010; Nagakura et al. 2010) that bright light curves can be produced by photospheric radiation. Comparing the light curves at different angles we see that there seem to be a sharp difference between the light curves at off-axis angles $\theta_o < 3$ and those at $\theta_o > 3$. The inner light curves have a bright early phase, characterized by some level of variability, while the outer light curves have a dim early phase, becoming more luminous at times when the inner light curves have lost their brightness. The inner light curves are bright during the “shocked jet” phase, as discussed in Morsony et al. (2007), and become much more dim in the “unshocked jet” phase, during which they are flat and featureless (at $t \geq 40 \text{ s}$). This difference is due to the fact that during the “shocked jet” phase the jet is hydrodynamically squeezed and its opening angle is smaller than the injection opening angle, so that very little emission is seen at $\theta > \theta_j \sim 4^\circ$ (see Figure 6 of Morsony et al. 2010). We also note that the very sharp rise and decay times seen in the on-axis light curve are not present in the off-axis ones. We conclude that the $\theta_o = 0^\circ$ light curve is affected by 2D numerical artifacts and its temporal shape should not be taken as conclusive. We finally note that the sharp turn-off of the light curves at $t \sim 95 \text{ s}$ is due to the fact that we turned off the engine at $t = 100 \text{ s}$ ⁶, and is therefore an artifact of our choice for the engine duration.

⁶ The $\sim 5 \text{ s}$ difference is the time it takes the jet to break out of the progenitor star.

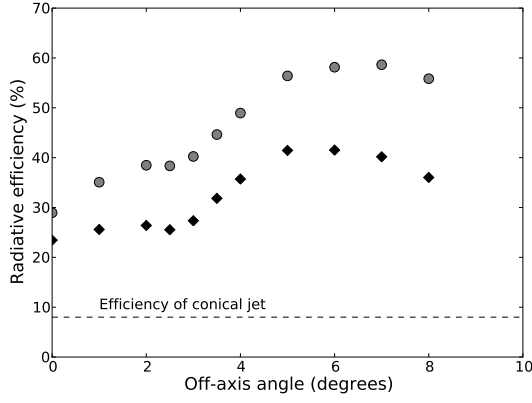


FIG. 3.— Radiative efficiency of the photosphere's radiation as a function of the off-axis observer. Gray symbols show results extracted directly from the simulations, while black diamonds show the result when the correction for the finite simulation box is applied.

An important conclusion we reached in paper I was that of the large radiative efficiency of the photospheric emission. The radiative efficiency is computed as the ratio between the energy that is radiated at the photosphere and the total kinetic energy in the flow just below the photosphere. In this paper we confirm our previous finding, even though we point out that the efficiency computation is severely affected by the finite size of the computation box. Figure 3 shows the efficiency computed directly from the simulation (gray circles) and the one derived by applying the finite box correction (Eq. 5). The efficiencies computed in the two ways are different by a factor ~ 2 . In any case, even the lower estimate puts the efficiency of the photospheric emission in the 30% range, larger than any efficiency that can be obtained in internal shocks, without assuming an ad-hoc broad distribution of Lorentz factors (Lazzati et al. 1999; Panaitescu et al. 1999). The figure also shows the photospheric efficiency for a conical jet with the same initial conditions that we adopted in our simulation (8%). Our simulation shows that the jet coupling with the progenitor star material has the effect of increasing the photospheric efficiency by a factor 3 to 8, with the highest increase observed at relatively large off-axis angles (3 to 8 degrees). The efficiency seems to have a somewhat bimodal behaviour, with the light curves for $\theta_o < 4^\circ$ having a $\sim 30\%$ efficiency and the light curves for $\theta_o > 4^\circ$ have a $\sim 50\%$ efficiency. The difference of light curves between small and large angles has been noted above. It seems that at small angles the light curve is dominated by the emission from the shocked-jet phase (Morsony et al. 2007), with an efficiency of $\sim 30\%$. At larger off-axis angles, however, the emission is dominated by the phase during which the jet enters the corresponding line of sight. In this case the photospheric efficiency is larger, probably as a consequence of the dissipation due to the shearing motion of the jet with the progenitor star material.

Another parameter we extracted from the simulations is the peak frequency of the light curves (Eq. 3). Figure 4 shows the result of the temporal evolution of the peak frequency for the various lines of sight. First, we note that the observed peak frequencies are in fairly good agreement with the peak frequencies observed in GRBs, with an observed mode $h\nu_{\text{obs}} = 250$ keV (Kaneko et al. 2006). A moderate hard-to-soft evolution is observed for the $\theta_o = 0^\circ$ curve. This is intriguing, given the so far unexplained hard-to-soft trend in many GRBs. However it could be an artifact of the $\theta_o = 0^\circ$ line of sight, since the trend is not observed at larger off-axis

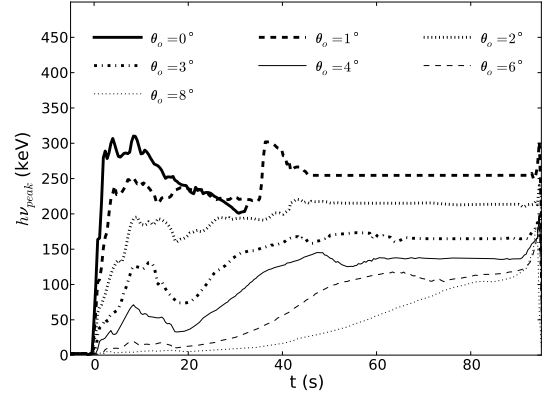


FIG. 4.— Temporal evolution of the peak frequency of the light curves for the various off-axis angles. The $\theta_o = 0^\circ$ curve is shown only for the first 33 seconds, since a sudden increase to a peak frequency of ~ 700 keV is seen afterwards. This sudden increase is due to the onset of the unshocked jet phase (Morsony et al. 2007), but the actual value of the peak frequency is a numerical artifact due to the coincidence of the line of sight with the symmetry axis of the simulation.

angles. The comparison of the outer light curves ($\theta_o > 3^\circ$) with their peak frequency evolution suggests the presence of tracking behaviour, i.e., increasing peak frequency when the light curve brightens and decreasing peak frequency when the light curve dims. This behavior is shown in Figure 5 for the $\theta_o = 4^\circ$ light curve.

A fundamental aspect of the observed GRB spectrum is the presence of non-thermal power-law tails at either end of the spectrum. The origin of the high-frequency tail in photospheric emission has been widely investigated and it has been shown that whenever some level of dissipation is present in the sub-photospheric region ($10 < \tau_T < 1$), inverse Compton processes produce a power-law tail comparable to the observations, extending up to tens or hundreds of MeV (Pe'er et al. 2005, 2006; Giannios 2006; Giannios & Spruit 2007; Lazzati & Begelman 2010; Beloborodov 2010). A more serious problem for photospheric emission models is the presence of non-thermal low-frequency tails. If the spectrum is generated in a 1-zone photospheric model with radiation and matter in thermal equilibrium, non-thermal low-frequency spectra are prohibited since they would violate the Raleigh-Jeans limit. Pe'er & Ryde (2010) explored the possibility of producing low-frequency non-thermal tails by considering the multi-color black body spectrum integrated over the emitting surface. They conclude that flat low-frequency spectra comparable to those observed can be indeed produced by multi-color photospheres, but only during the decaying part of the light curve. Pe'er and Ryde (2010) considered emission from conical jets, for which analytic predictions can be made. We have computed the multi-color spectrum from our simulations to check whether a non-thermal spectrum at low-frequencies can be obtained during the raising part of the light curve, relaxing the conical jet approximation. The resulting spectrum is shown in Figure 6, compared to a thermal spectrum with the same peak frequency (dashed line). As the figure shows, we do not find any significant deviation from a Planck law, because the emission is dominated by the parcel of the outflow that moves towards the observer. This conclusion is not in disagreement with the calculation of Pe'er & Ryde (2010), since they could find deviations from a thermal spectrum only when the material pointing directly at the observer is not producing any radiation.

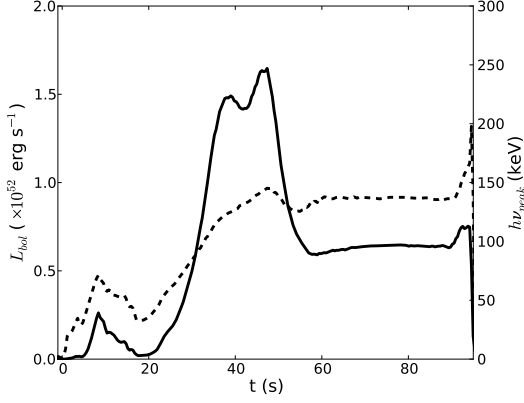


FIG. 5.— Photospheric light curve for the $\theta_o = 4^\circ$ line of sight (solid line, left y axis) compared to the evolution of the peak frequency of the spectrum (dashed line, right y axis).

4. A QUANTITATIVE COMPARISON

In order to better evaluate the role of photospheres in the production of the prompt GRB radiation, we attempt a quantitative comparison of our results with spectral and luminosity data. It is well known that observed GRBs for which a redshift measurement is available obey to the Amati correlation (Amati et al. 2002). According to this correlation, the burst frame peak frequency is correlated with the total isotropic equivalent luminosity elevated to an exponent close to 0.5. The most recent best fit to the correlation reads:

$$h\nu_{\text{peak}} = 102 \left(\frac{E_{\text{iso}}}{10^{52} \text{erg s}^{-1}} \right)^{0.54} \quad (7)$$

(Amati, private communication), where the peak frequency is expressed in keV. The dispersion of the data around the best fit line is Gaussian with a sigma of 0.2. Figure 7 shows the best fit correlation with a dashed line and the $3-\sigma$ dispersion areas with dotted lines. The location of our light curves in the Amati plane is shown with gray circles (calculated directly from the simulation) and black diamonds (after the finite box correction). The simulation points are connected with a line showing the evolution from the on-axis light curve (upper right point) to the most off-axis light curve (lowest left point).

The comparison of the simulated light curves with the Amati correlation is contradictory. On the bright side, as the observer moves away from the jet axis, the isotropic energy and peak frequency evolve in such a way as to reproduce the slope of the correlation. This is independent of whether we consider the corrected or uncorrected light curves as the most reliable result. On the other hand, the normalization is incorrect, since the simulated light curves are too bright for the corresponding peak frequency (see also Nagakura et al. 2010).

5. DISCUSSION

This paper presents the natural extension of our 2009 numerical study of the photospheric emission from long-duration GRB jets (paper I). We here present a simulation run on a domain ten times bigger than in paper I. Such a simulation allows us to explore the location, spectrum, and light curves of photospheres along lines of sight different from the jet axis. The results of this paper substantially confirm the results of paper I, even though we find that some details of paper I had been affected by the relatively small computational domain and by the coincidence of the line of sight with the symmetry axis of the computation. For example, the sharp

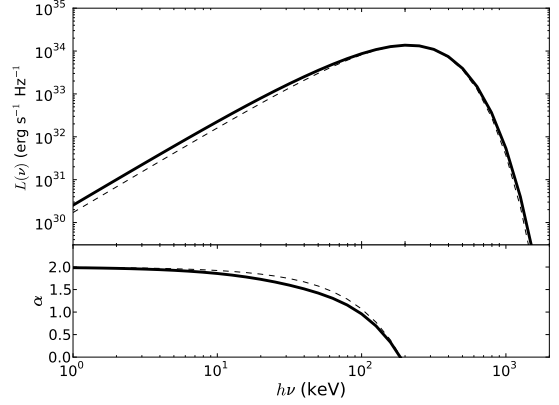


FIG. 6.— Observed spectrum for the $\theta_o = 1^\circ$ observer at $t = 30$ s, integrated over the emitting surface (upper panel, thick solid line). The spectrum shows only small deviations with respect to a Planck function with the same maximum (thin dashed line). The bottom panel shows the local power-law slope of the two spectra ($L(\nu) \propto \nu^\alpha$), emphasizing that the difference in the slopes is very small.

features seen in the on-axis light curve disappear as soon as the observer moves away from the jet axis. However, we find that the high efficiency of the photospheric radiation is confirmed and that the efficiency increases for off-axis lines of sight.

Even with the big simulation box presented here ($Z_{\text{out}} = 2.5 \times 10^{13}$ cm), the photosphere during some times interval is sometimes affected by the box size. We therefore discuss a correction that allows us to derive the correct location of the photosphere under the approximation of self-similar non-accelerating expansion beyond the box outer edge. Off-axis photospheric light curves were discussed elsewhere (Mizuta et al. 2010; Nagakura et al. 2010). Mizuta et al. perform a simulation with an identical setup to our paper I. They derive off-axis light curves and spectra, but their simulation box has an outer edge $Z_{\text{out}} = 2.5 \times 10^{12}$ cm, making their results unreliable. In fact, our Figure 2 shows that for all lines of sight the photosphere is well outside their simulation box. Nagakura et al. (2010) perform instead a somewhat low-resolution simulation extending to very large radii. While their simulation is superior to the one we present here in terms of size, their resolution and the adoption of a fixed-grid algorithm make their results inaccurate in terms of the internal properties of the outflow. In particular, a fixed-grid algorithm is not able to resolve the tangential shocking that we observe in the jet out to hundreds of stellar radii, losing the dissipation due to such shocks and therefore underestimating the temperature at the photosphere.

The size of this simulation box allows us to perform an interesting comparison between the physically motivated photospheric light curves and the light-power curves that we have used in other publications as proxies to the real light curve (Lazzati et al. 2010ab; Morsony et al. 2010). The comparison is shown in Figure 8 for the $\theta_o = 1^\circ$ line of sight. Light-power curves were extracted at radii of 10^{11} and 10^{13} cm, assuming an efficiency of 30%. We find that in all cases the three bolometric light curves show a strong correlation, demonstrating that the use of light-power curves is justified. However, the light-power curve extracted at the largest radius does show a bright early spike that is not present in the other curves. This spike is due to the presence of slow, dense material that piles up ahead of the jet and it may well be an artifact of the presence of a reflecting boundary condition along the jet axis.

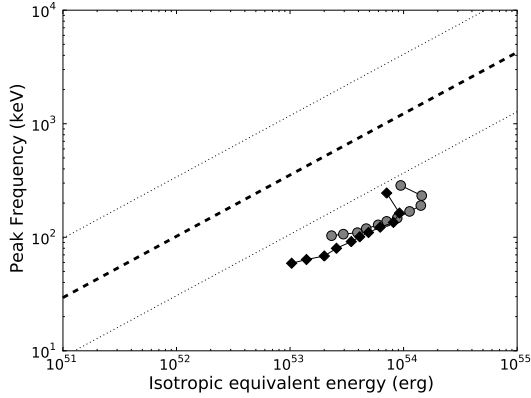


FIG. 7.— Location of our simulated photospheric light curves and spectra in the Amati diagram. The dashed line shows the location of the best-fit Amati relation, while the dotted lines show the $3-\sigma$ dispersion around it. Black and gray symbols show the results with and without the finite-box correction, respectively.

The comparison of photospheric light curves with light-power curves at different off-axis angles produces results in qualitative agreement with what shown for the $\theta_o = 1^\circ$ case.

Two of our new and more interesting results (not discussed in paper I) concern the spectrum of the photospheric emission. First, we find that the integration of the multi-color black-body spectrum over the emitting surface does not alter substantially the Planck law shape of the photospheric emission (Figure 6). Second, we find that the peak frequencies produced by the photosphere are too small for the isotropic equivalent energy of their respective light curves (Figure 7). These two results are important because they show that the photospheric emission has trouble in reproducing the non-thermal low-frequency spectra observed in GRBs and their peak frequencies. Both these problems may be solved if the assumption of thermal equilibrium between the baryons and the radiation field that we adopted to derive the spectrum are inadequate. As a matter of fact, the bolometric light curve calculation relies on the simple assumption that the internal pressure of the outflow is mainly due to radiation and is therefore quite robust. Such assumption is correct no matter the spectrum of the radiation field. If, however, the radiation has a color temperature that is higher than its effective temperature, our spectral calculations would be incorrect. A first consequence would be that the peak frequency that we derive is underestimated, and therefore the Amati correlation discrepancy could disappear. As a matter of fact, in scattering dominated accretion disk atmospheres, a discrepancy of a factor ~ 3 is found

in detailed radiation transfer calculations (e.g., Davis et al. 2005). In addition, having a color temperature higher than the effective temperature, allows for the presence of non-thermal low-frequency tails without violating the Rayleigh-Jeans limit.

Even though finding the exact mechanism that would create such an off-balance configuration between the baryon and the radiation field is beyond the scope of this paper, we argue that research on the photospheric emission of GRB jets should proceed in two directions. On the one hand, it is mandatory to explore the shape of the spectrum of the photospheric emission from first principles, relaxing the assumption of equilibrium. On the other hand, the role of different jet and progenitor properties should be explored, since all the available simulations have so far concentrated on the progenitor model 16TI (Woosley & Heger 2006) and on jet configurations analogous to the one we explored in paper I.

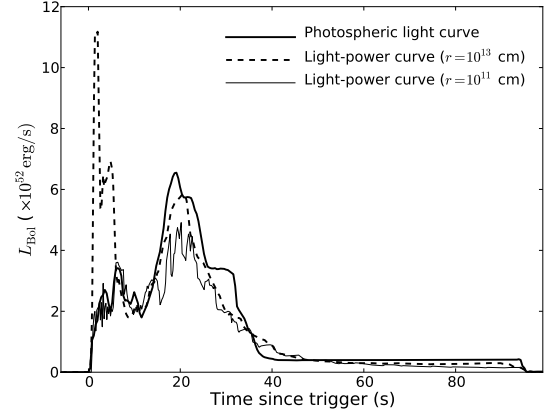


FIG. 8.— Comparison between the $\theta_o = 1^\circ$ photospheric light curve (thick solid line) and light-power curves extracted at the same viewing angle at radii $r = 10^{13}$ cm (thick dashed line) and $r = 10^{11}$ cm (thin solid line).

We thank Kris Beckwith for useful discussions and Lorenzo Amati for providing us with an updated version of his correlation. Resources supporting this work were provided by the NASA High-End Computing (HEC) Program through the NASA Advanced Supercomputing (NAS) Division at Ames Research Center. The software used in this work was in part developed by the DOE-supported ASC / Alliance Center for Astrophysical Thermonuclear Flashes at the University of Chicago. This work was supported in part by NASA ATP grant NNG06GI06G, Fermi GI program NNX10AP55G and Swift GI program NNX08BA92G.

REFERENCES

- Abdo, A. A., et al. 2009, *Science*, 323, 1688
 Amati, L., et al. 2002, *A&A*, 390, 81
 Baring, M. G., & Braby, M. L. 2004, *ApJ*, 613, 460
 Beloborodov, A. M. 2010, *MNRAS*, 407, 1033
 Davis, S. W., Blaes, O. M., Hubeny, I., & Turner, N. J. 2005, *ApJ*, 621, 372
 Fryxell, B., et al. 2000, *ApJS*, 131, 273
 Ghisellini, G., & Celotti, A. 1999, *ApJ*, 511, L93
 Ghisellini, G., Ghirlanda, G., Nava, L., & Celotti, A. 2010, *MNRAS*, 403, 926
 Giannios, D. 2006, *A&A*, 457, 763
 Giannios, D., & Spruit, H. C. 2007, *A&A*, 469, 1
 Goodman, J. 1986, *ApJ*, 308, L47
 Kaneko, Y., Preece, R. D., Briggs, M. S., Paciesas, W. S., Meegan, C. A., & Band, D. L. 2006, *ApJS*, 166, 298
 Kumar, P., & Barniol Duran, R. 2009, *MNRAS*, 400, L75
 Lazzati, D., Ghisellini, G., & Celotti, A. 1999, *MNRAS*, 309, L13
 Lazzati, D., Ghisellini, G., Celotti, A., & Rees, M. J. 2000, *ApJ*, 529, L17
 Lazzati, D., Morsony, B. J., & Begelman, M. C. 2009, *ApJ*, 700, L47
 Lazzati, D., & Begelman, M. C. 2010, *ApJ*, 725, 1137
 Lazzati, D., Morsony, B. J., & Begelman, M. C. 2010a, *ApJ*, 717, 239
 Lazzati, D., Blackwell, C. H., Morsony, B. J., & Begelman, M. C. 2010b, *MNRAS* in press (arXiv:1008.4364v2)
 Lloyd, N. M., & Petrosian, V. 2000, *ApJ*, 543, 722
 Mizuta, A., Nagataki, S., & Aoi, J. 2010, *ApJ* submitted (arXiv:1006.2440v2)
 Morsony, B. J., Lazzati, D., & Begelman, M. C. 2007, *ApJ*, 665, 569
 Morsony, B. J., Lazzati, D., & Begelman, M. C. 2010, *ApJ*, 723, 267
 Nagakura, H., Ito, H., Kiuchi, K., & Yamada, S. 2010, *ApJ* submitted (arXiv:1009.2326v1)
 Panaitescu, A., Spada, M., & Mészáros, P. 1999, *ApJ*, 522, L105
 Pe'er, A., & Waxman, E. 2004, *ApJ*, 613, 448
 Pe'er, A., Mészáros, P., & Rees, M. J. 2005, *ApJ*, 635, 476

- Pe'er, A., Mészáros, P., & Rees, M. J. 2006, ApJ, 642, 995
Pe'er, A., & Ryde, F. 2010, ApJ submitted (arXiv:1008.4590v1)
Piran, T. 1999, Phys. Rep., 314, 575
Rees, M. J., & Mészáros, P. 2005, ApJ, 628, 847
Woosley, S. E., & Heger, A. 2006, ApJ, 637, 914
Zhang, B., & Yan, H. 2010, ApJ in press (arXiv:1011.1197v1)